

Horseshoe orbits for the elliptic restricted three-body problem

Elan Gin * P. W. Sharp †

February 25, 2005

Abstract

Symmetric horseshoe orbits for the circular restricted three-body problem (R3BP) have been well studied. Little is known about horseshoe orbits for the more general and more realistic elliptic problem. We present families of such orbits for the planar elliptic problem with the Jupiter-Sun mass ratio. The families bifurcate from orbits for the circular problem and they all have a turning point in the eccentricity. These turning points lead to new families of horseshoe orbits for the circular problem which lead to new circular-elliptic bifurcations and so on. Continuation in the eccentricity thus proves an effective way to find new families for the circular problem.

We also investigate the orbital and vertical stability along with the three-dimensional bifurcations of the new elliptic orbits, particularly for eccentricities in a small range about that for Jupiter. We find three-dimensional bifurcations are possible in this range, showing the dynamics of horseshoe orbits in the Sun-Jupiter system could be appreciably more complex than modelled by the circular R3BP.

Keywords: restricted three-body problem, elliptic, horseshoe, bifurcations

MR 2000: 70F10

1 Introduction

The restricted three-body problem (R3BP) has long been used to model the orbital motion of two massive bodies, known as primaries, and a third body of very small mass. Much is known about the solutions to the R3BP and it has many applications including those described in [1], [2], [4], [7], [8], [10], [12], [13], [17], [19], [20], [21] and [24, 25].

Of particular interest because of their applications, see for example [8], [10], [20] and [21], are symmetric horseshoe orbits. These are periodic symmetric orbits encircling the Lagrangian points L_3 , L_4 and L_5 . Two contrasting horseshoe orbits are depicted in Figure 1. The left horseshoe has a smooth outer edge and two loops in its inner edge; the right horseshoe has loops on both edges. Other horseshoe orbits are depicted in Figure 4.

*Department of Mathematics, University of Auckland, Private Bag 92019, Auckland, New Zealand. Email: elan@math.auckland.ac.nz

†Same address as the first author. Email: sharp@math.auckland.ac.nz

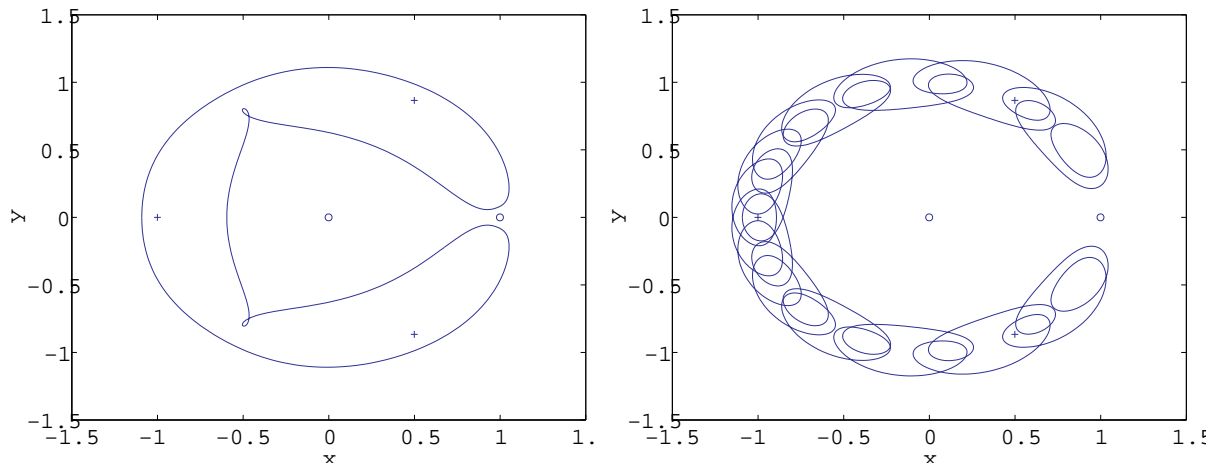


Figure 1: Two possible horseshoe orbits for the Sun-Jupiter system. The Sun and Jupiter are denoted by a circle, with the Sun near the origin and Jupiter near $x = 1$. The plus signs denote the Lagrangian points L_3 (negative x), L_4 (first quadrant) and L_5 (fourth quadrant).

Horseshoe orbits for the circular R3BP have been well studied, see for example Schanzle [18], Rabe [15] and Taylor [19]. Little is known about horseshoe orbits for the more general and more realistic elliptic R3BP. We present families of orbits for the Jupiter-Sun mass ratio that bifurcate from horseshoe orbits for the circular problem and investigate their stability and three-dimensional bifurcations. The Jupiter-Sun mass ratio was chosen because of the importance of Jupiter in the dynamics of the Solar System.

In the circular problem, the period T of the massless particle can potentially be any positive value. In the elliptic problem, T must be an integer multiple of the period of the two primaries which in the standard, non-dimensionalised units we use is 2π . Although restrictive, this requirement on T suggests a technique for finding bifurcations of horseshoe orbits for the circular and elliptic problems - continue a family of horseshoe orbits for the circular problem until an orbit with T an integer multiple of 2π is located.

We applied this technique to the seven families of horseshoe orbits of Taylor [19]. We continued the families further than in [19] and discovered fourteen circular-elliptic bifurcations. Each continuation was stopped when the intricacies of the orbits meant a prohibitive amount of CPU time was required to continue further. Our continuations are summarised in §2.

Once we had located the bifurcations, we used continuation on the orbital eccentricity of the primaries to follow the emanating family of elliptic orbits. As we show in §3, these continuations led to further families of horseshoe orbits for the circular problem, which led to further families of horseshoe orbits for the elliptic problem and so on. We then investigated the stability and three-dimensional bifurcations of the new elliptic orbits, especially for eccentricities in a small interval about that for Jupiter¹. Our investigation is summarised in §4. We end in §5 with a discussion of our work.

We used two predictor-corrector schemes for the continuation. The first had an initial

¹We used a small interval and not Jupiter's exact value (0.048) because of the approximations inherent in the R3BP and the (small) long-term variation in Jupiter's eccentricity.

condition or the eccentricity as the continuation parameter and a cubic predictor (a lower degree predictor was used for the first four orbits). The second scheme had pseudo-arclength as the continuation parameter and an Eulerian predictor. The corrector for both scheme was Newton's method applied to the conditions for periodicity. The first scheme was more efficient than the second but could not handle turning points. We began each continuation with the first scheme, changed to the second scheme to pass a turning point and then switched back to the first scheme.

Both schemes used an adaptive strategy for the continuation stepsize. The stepsize was halved if the corrector required five or more interactions to converge, doubled if three or fewer iterations were required and unchanged if four iterations were required. Newton's method was deemed converged if the error in the conditions for periodicity was less than 10^{-6} . The error for most orbits was several orders of magnitude smaller; the exact error depended on the stability of the orbit and the accuracy of the initial estimate. If the maximum number of ten iterations was reached without convergence, the continuation stepsize was halved and the problem re-attempted.

In other respects, our continuation schemes are similar to those commonly used on the R3BP, see for example Zagouras and Markellos [22], Zagouras and Perdios [23], and Katsiaris [9]. The state and variational equations were integrated using the order eight variable-step explicit Runge-Kutta method of Prince and Dormand [14].

We solved the state equations for the elliptic problem in the standard pulsating and rotating frame of reference with the true anomaly ν as the independent variable. The state equations for the planar (two-dimensional) problem consist of the equations for x and y , and are

$$\begin{aligned} \frac{d^2x}{d\nu^2} - 2\frac{dy}{d\nu} &= \frac{r}{p} \left[x - \frac{(1-\mu)(x+\mu)}{r_1^3} - \frac{\mu(x+\mu-1)}{r_2^3} \right], \\ \frac{d^2y}{d\nu^2} + 2\frac{dx}{d\nu} &= \frac{r}{p} \left[y - \frac{(1-\mu)y}{r_1^3} - \frac{\mu y}{r_2^3} \right], \end{aligned} \tag{1}$$

where μ is the mass ratio for the primaries, $p = 1 - \epsilon^2$, ϵ being the orbital eccentricity of the primaries, $r = (1 - \epsilon^2)(1 + \epsilon \cos \nu)^{-1}$, $r_1^2 = (x + \mu)^2 + y^2$ and $r_2^2 = (x + \mu - 1)^2 + y^2$. These equations reduce to those for the circular problem by setting $\epsilon = 0$ and replacing ν with the time t as the independent variable. We took $\mu = 0.000953875$ as the Jupiter-Sun mass ratio.

Orbital instability (see §4) meant it was impossible to follow some families of circular orbits as accurately or as far as we wanted using double precision (16 digit arithmetic), and we resorted to quadruple precision (32 digit arithmetic). Quadruple precision is 21 times slower than double precision on our computer and its use meant some of our runs required several days of CPU time.

2 Taylor's seven families

Rabe [15] gave some horseshoe orbits for the circular problem with the Jupiter-Sun mass ratio and conjectured there was a family of such orbits. The initial conditions for the

orbits were chosen so $y(0) = \dot{x}(0) = 0$ which meant the orbits were symmetric about the x -axis. Taylor [19] greatly extended this work by showing there existed many, possibly infinitely many, families of (symmetric) horseshoe orbits that could be followed by using continuation on $x(0)$. Taylor gave representative orbits from seven families and described how the stability and the number of loops on the inner and outer edges varied along these families.

The orbits given in Tables 1, 2 and 3 of Taylor [19] and listed here in Table 1 were used as the starting points for our initial continuations on $x(0)$. For each orbit of each continuation, $\dot{y}(0)$ was found by solving the periodicity condition and T was defined by the time of crossing of the x -axis; $y(0)$ and $\dot{x}(0)$ were zero for all orbits.

Family	$x(0)$	$\dot{y}(0)$	$T/(2\pi)$
$h(9, 8)$	-1.09147	0.13205	9.3878
$h(9, 9)$	-1.05828	0.07617	10.4102
$h(10, 11)$	-1.07931	0.11627	12.3840
$h(13, 14)$	-1.06857	0.10140	15.3692
$h(16, 17)$	-1.05691	0.08350	18.3366
$h(20, 21)$	-1.03136	0.04083	22.2728
$h(27, 28)$	-1.02680	0.03897	29.1966

Table 1: Starting orbits for our initial continuations on $x(0)$. The first column lists Taylor's nomenclature for the families. The remaining columns list $x(0)$, $\dot{y}(0)$ and $T_s = T/(2\pi)$.

Figure 2 gives the graphs of $T_s = T/(2\pi)$ against $x(0)$ for each of the seven families. The integer values of T_s are labelled as kA where k is T_s and $A = a, b, \dots$, indicates for most cases the order the bifurcations for $T_s = k$ were located. The seven families were continued as far as numerically feasible. The general shape of all families except for $h(9, 9)$ is similar in that T_s appears to asymptotically approach an integer value at the rightmost end. For $h(9, 8)$, $h(9, 9)$, $h(10, 11)$, $h(13, 14)$ and $h(20, 21)$ both ends of the families depicted in Figure 2 have not terminated but further continuation would have required prohibitive amounts of CPU time. For $h(27, 28)$ the leftmost end of the branch has terminated. The loops of the orbits near this endpoint enlarged until they started to coincide. Further continuation led to the loops collapsing onto a single loop. This loop became smaller until it enclosed L_1 only, thus no longer a horseshoe orbit. This behaviour had been reported by Schanzle [18] who noticed this collapse occurred for $x(0) = -2$. Taylor [19] conjectured such a collapse would happen for $h(27, 28)$ at both ends of the family and the resulting orbits would be members of a different family.

We conjecture from the shape of the solution reached that a similar collapse occurs for $h(16, 17)$.

As we move right to left along the $T_s(x(0))$ curves for $h(9, 8)$, $h(10, 11)$, $h(13, 14)$ and $h(20, 21)$, we observe a turning point in $x(0)$ at the first approach to $x(0) = -2$. This leads to a second and in three cases, a third integer value for T_s .

Family $h(9, 9)$ is unique among the seven families in having no integer values for T_s .

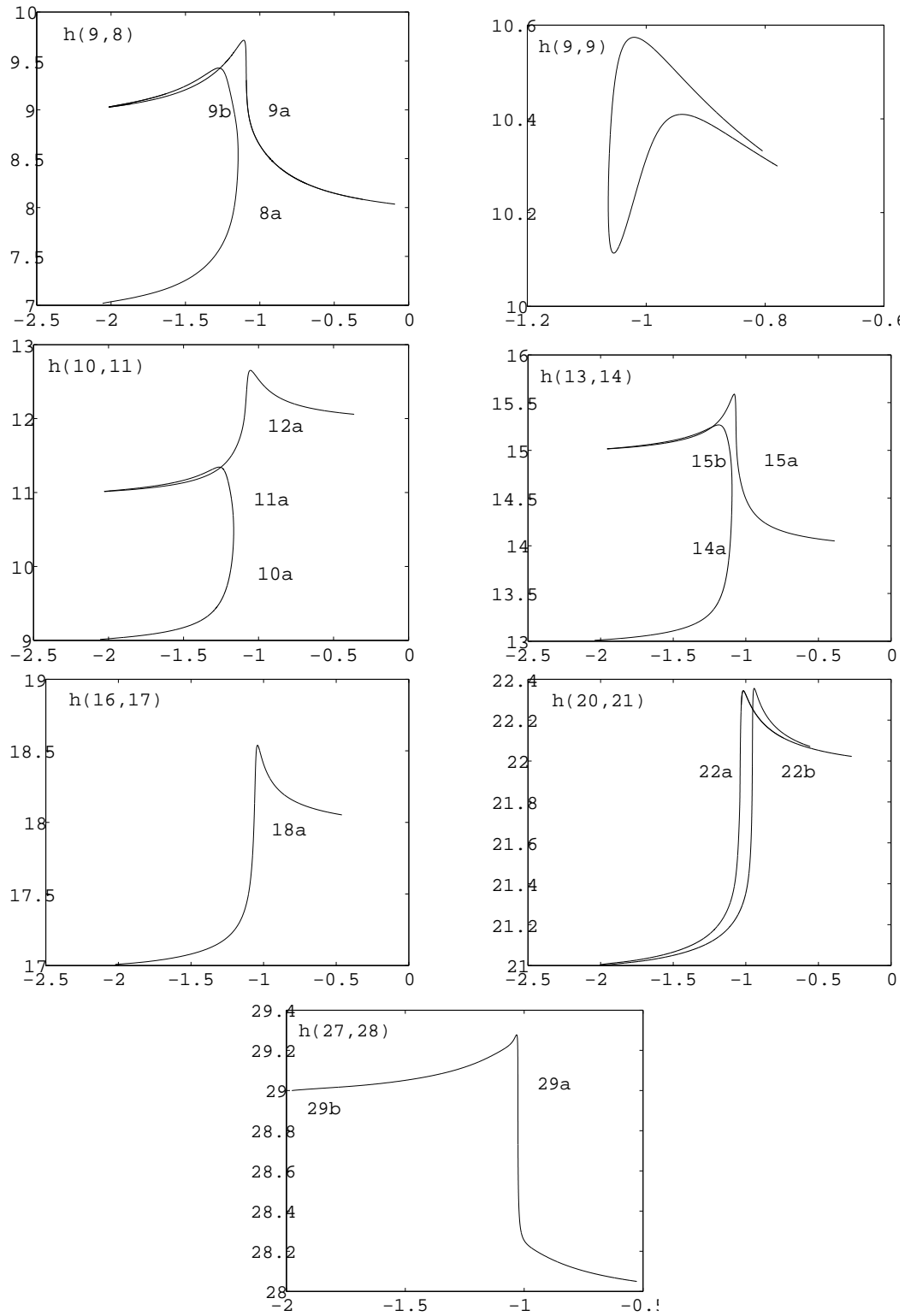


Figure 2: The scaled period T_s as a function of $x(0)$ for each of Taylor's seven families. The vertical axis gives T_s and the horizontal axis $x(0)$. The integer values of T_s are labelled.

3 Continuation on ϵ for $h(9, 8)$

We had intended to present continuations on ϵ for each of the fourteen circular-elliptic bifurcations identified in the previous section. We began with the bifurcations for $h(9, 8)$ and found the resulting structure was appreciably richer than we expected, making it impractical to present the results for all bifurcations.

The orbits 9a, 9b and 8a were taken as starting points for continuation on the eccentricity ϵ . We first describe the findings for 9a and 9b. Figure 3 gives the families of solutions found. We observe for 9a that ϵ does not increase monotonically towards

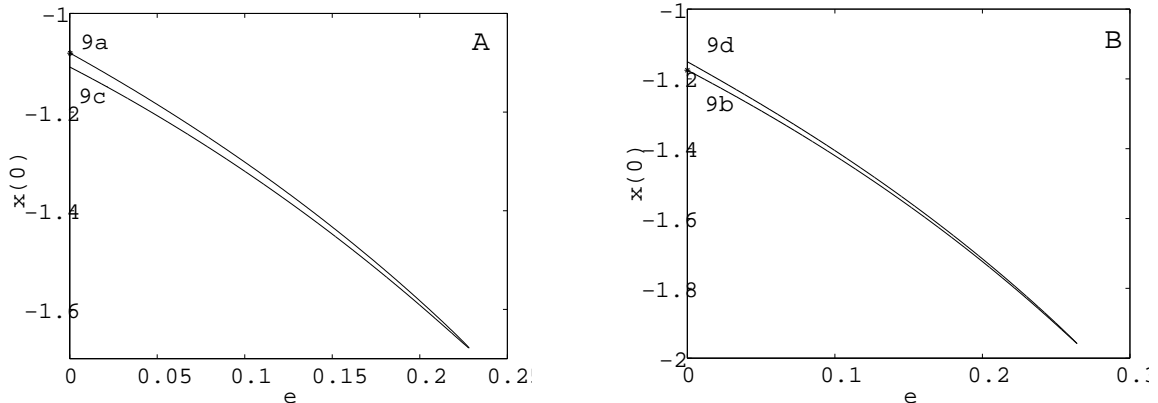


Figure 3: Continuation on ϵ : A - from 9a, B - from 9b.

one. Instead there is a turning point at $\epsilon \approx 0.228$ and ϵ returns to zero to give a new circular-elliptic bifurcation. We label the circular orbit at this bifurcation 9c. A similar thing happens with 9b, giving a new circular orbit we label 9d. In both cases, there is the possibility of a new family of circular orbits. We return to this point later.

Figure 4 illustrates changes in the orbits along the curve 9a-9c. As ϵ increases, the orbit forms six outer loops and the two inner loops become larger. These loops enlarge with increasing ϵ . After ϵ reaches its maximum value, the loops shrink and eventually disappear to give a smooth outer curve when $\epsilon = 0$. We also observe that as ϵ increases, $x(0)$ becomes more negative and the two arms of the horseshoe orbit start to cross at $\epsilon \approx 0.210$. This crossing means the particle of infinitesimal mass makes very close approaches to Jupiter.

We next performed a continuation on $x(0)$ starting with the two new circular orbits 9c and 9d. We found the branches through 9c and 9d join. Hence while 9c and 9d are different circular orbits, they are of the same family. We also found another orbit with $T_s = 8$, we label this orbit 8c, and a turning point at $x(0) \approx -2$. Figure 5 gives the curve $T_s(x(0))$ and the location of 8c.

Plot A in Figure 6 depicts the continuation on ϵ from orbit 8a. As before, ϵ had a turning point, this time at $\epsilon \approx 0.616$, and upon return to $\epsilon = 0$ we obtained a new orbit with $T_s = 8$. We label this orbit 8b.

We took orbit 8b and continued on $x(0)$ to trace out a family for the circular problem, see Plot B, Figure 6. This continuation led to an orbit with $T_s = 7$. We label this orbit

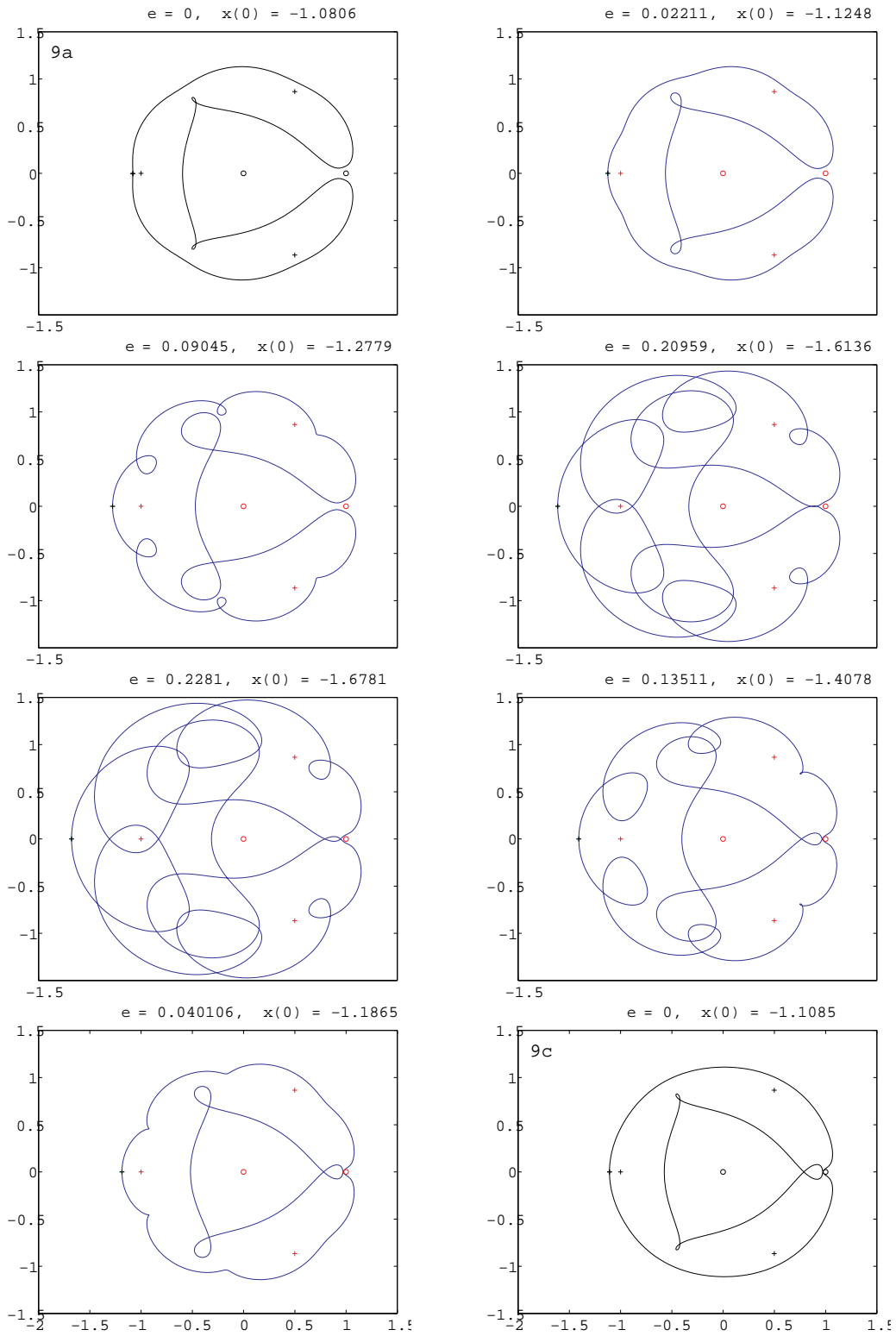


Figure 4: Evolution of the orbits as ϵ increases and then decreases along 9a-9c. The horizontal axis is x and the vertical axis y .

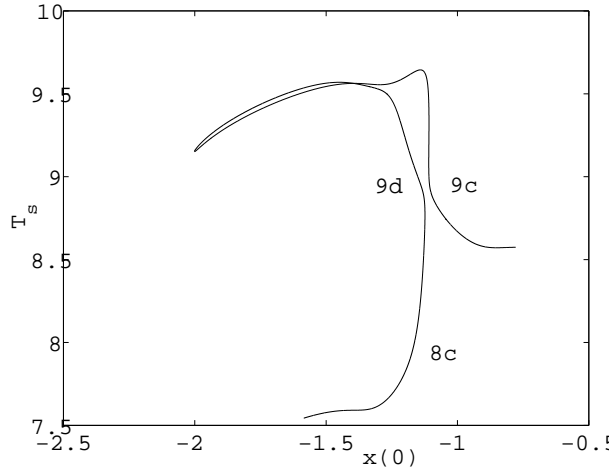


Figure 5: T_s vs $x(0)$. This curve was found by continuation on $x(0)$ from 9c and 9d.

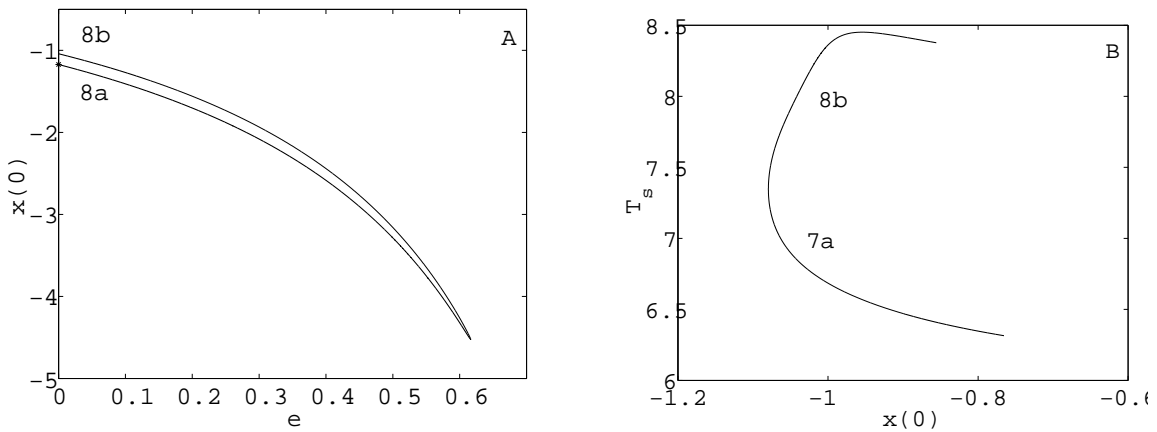


Figure 6: A - continuation on ϵ from 8a; B - continuation on $x(0)$ from 8b.

7a. We then continued on ϵ from orbit 7a to find solutions for the elliptic problem with $T_s = 7$. This family is given in Plot A, Figure 7. This continuation found another orbit for $T_s = 7$, we label this orbit 7b. We next used continuation on $x(0)$ to find the family containing 7b, see Plot B, Figure 7. The continuation produced a third orbit with $T_s = 8$. We label this orbit 8e (and not 8d because we anticipate a continuation on ϵ from 8c would give a new circular orbit 8d).

The relationship between the orbits for integer values of T_s found by continuation on ϵ and $x(0)$ are summarised in Figure 8. The initial values for the orbits in Figure 8 are given in Table 2.

We observe by comparing the $T_s(x(0))$ curves in Figures 5, 6 and 7 with those in Figure 2 that the families of circular horseshoe orbits containing 7a, 7b, 8b, 8c, 8e, 9c and 9d are different from Taylor's seven families. Thus continuation in ϵ has provided an effective way to find new families of circular horseshoe orbits. Zagouras and Perdios [23] used a similar approach to find periodic orbits for the planar circular problem. They

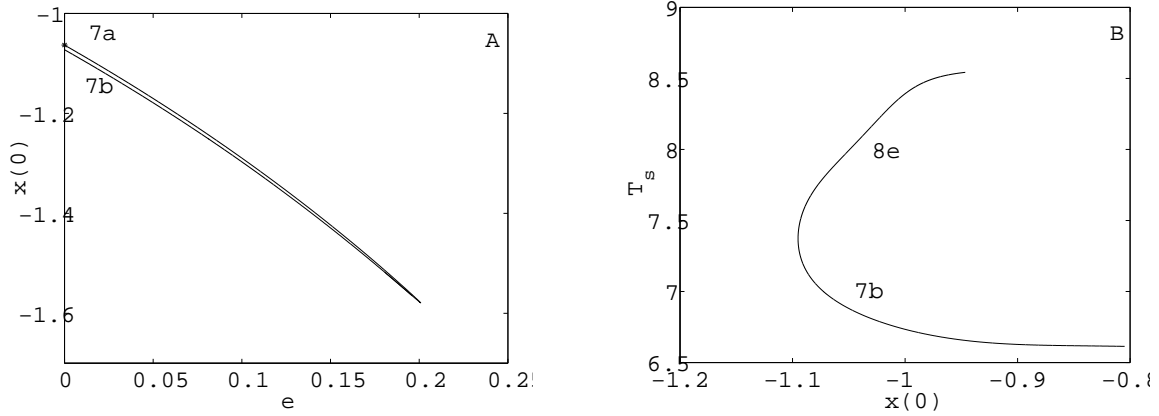


Figure 7: A - continuation on ϵ from 7a; B - continuation on $x(0)$ from 7b.

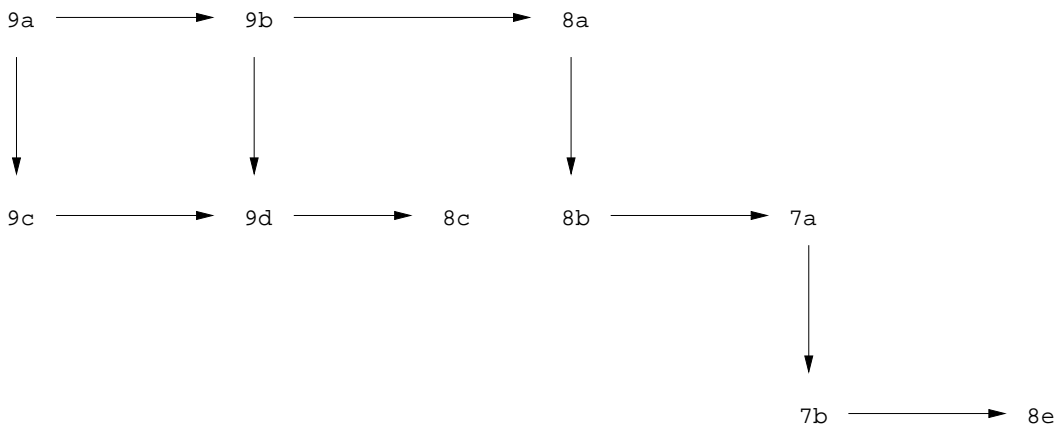


Figure 8: The horizontal and vertical lines represent continuation on $x(0)$ and ϵ respectively. The length of the arrows is immaterial.

Orbit	$x(0)$	$\dot{y}(0)$
9a	-1.079981	0.108206
9b	-1.175110	0.278948
9c	-1.110849	0.159983
9d	-1.150879	0.236022
8a	-1.172541	0.270077
8b	-1.041666	0.018151
8c	-1.163723	0.253041
8e	-1.049192	0.032854
7a	-1.063201	0.055933
7b	-1.072533	0.072576

Table 2: The initial conditions for some circular-elliptic bifurcation orbits.

found three-dimensional periodic orbits through an ascent from families of planar orbits; the subsequent descent to the plane found new families for the planar case. Zagouras

and Perdios describe this an efficient way to locate new families of orbits for the planar circular problem.

4 Linear stability analysis

In this section we give a brief review of vertical and orbital stability for the planar problem and present a summary of these stabilities for the families of elliptic orbits 9a-9c, 9b-9d, 8a-8b and 7a-7b.

The concept of vertical stability was introduced by Hénon [6] for the circular planar problem. This type of linear stability examines the growth of perturbations perpendicular to the $x - y$ plane and is measured using the parameter s_v . An orbit is vertically stable if $|s_v| < 1$ and vertically unstable if $|s_v| > 1$. If $s_v = 1$, there is a bifurcation with a three-dimensional orbit of the same multiplicity (the number of crossings of a prescribed plane or axis) as the planar orbit; if $s_v = -1$, there is a bifurcation with a three-dimensional orbit of twice the multiplicity. Zagouras and Markellos [22] discuss these types of bifurcations in more detail.

The parameter s_v can be calculated as follows, see for example Markellos [11]. The state equations for the planar problem are extended to those for the three-dimensional problem and then written as the six first-order equations $\dot{w}(t) = f(w(t))$ where $w = [x, y, z, \dot{x}, \dot{y}, \dot{z}]^T$ and z is the coordinate perpendicular to the $x - y$ plane. The variational equations for $w(0)$ are then

$$\dot{V} = \frac{\partial f(w)}{\partial w} V \quad (2)$$

where V is the 6×6 matrix defined as $v_{ij} = \partial f_i / \partial w_{0j}$, w_{0j} being $w_j(0)$. The state and variational equations are integrated from $t = 0$ to $t = T$ to give the monodromy matrix $V(T)$; the state equations are included because f depends on w . We then have

$$s_v = \frac{v_{33}(T) + v_{66}(T)}{2}. \quad (3)$$

As Robin [16] points out, the concept of vertical stability generalises to the elliptic problem, with the expression for s_v being the same as for the circular problem.

Orbital stability for the planar problem examines the growth of perturbations to the initial conditions $x(0)$, $y(0)$, $\dot{x}(0)$ and $\dot{y}(0)$. Thus orbital stability deals with perturbations in the plane and complements vertical stability.

Orbital stability for the circular problem is measured using the eigenvalues of the monodromy matrix. Bray and Goudas [3] derived necessary and sufficient conditions for a three-dimensional periodic orbit to be orbitally stable (one of these conditions was later corrected by Hadjidemetriou [5], p. 262). The derivation of [3] simplifies markedly for a planar orbit. Equation (74) in [3] for the relevant eigenvalues λ becomes $\phi(\lambda) = \lambda^2 + \alpha\lambda + 1$ where $\alpha = -\text{Tr}(V(T)) + 2$ and $V(T)$ is the monodromy matrix for the planar problem. Since the constant term in $\phi(\lambda)$ is 1, the two roots of ϕ must be reciprocals of one another. If the roots are real, whether distinct or equal, perturbations in the initial conditions will

in general grow with t . Hence stability requires the roots of ϕ be complex. This is equivalent to requiring

$$-2 < \alpha < 2. \quad (4)$$

Unlike vertical stability, the conditions for orbital stability for the circular and elliptic problems differ. Katsiaris [9] derived the conditions for orbital stability of the three-dimensional elliptic problem. For the planar elliptic problem, these conditions reduce to requiring $\phi(\lambda) = \lambda^4 + \alpha_1\lambda^3 + \alpha_2\lambda^2 + \alpha_1\lambda + 1$ has complex roots. This requirement is the same as that for orbital stability of the three-dimensional circular problem. Thus, the conditions for orbital stability of the planar elliptical problem are, see for example [22],

$$\Delta > 0, \quad |p| < 2, \quad |q| < 2, \quad (5)$$

where $\Delta = \alpha^2 - 4(\beta - 2)$, $p = (\alpha + \sqrt{\Delta})/2$, $q = (\alpha - \sqrt{\Delta})/2$, $\alpha = 2 - \text{Tr}(V(T))$, $\beta = (\alpha^2 + 2 - \text{Tr}(V^2))/2$.

The stability plots for 9a-9c, 9b-9d, 8a-8b and 7a-7b are shown in Figure 9. The left hand plots give s_v against ϵ and the right hand plots $\gamma \equiv \sinh^{-1}(\lambda_M)$ against ϵ where λ_M is the magnitude of the largest eigenvalue of $V(T)$. We used \sinh^{-1} for the ordinate in the right hand plots because of the large variation in λ_M and to induce a larger scale for λ_M near 1.

We observe from the left hand plots of Figure 9 that the curves for $s_v(\epsilon)$ for families 9a-9c, 9b-9d and 7a-7b are similar. A same observation holds for the curves for $\gamma(\epsilon)$. The curves for the remaining family (8a-8d) are noticeably different, particularly the curve for $\gamma(\epsilon)$.

All the orbits for family 8a-8b and most orbits for the remaining families have $|s_v| < 1$. Hence most orbits for the four families are vertically stable - a body perturbed out of the plane will return to the plane. The vertically unstable orbits do not have large values for $|s_v|$ and hence the vertical instability is mild.

Each of the families 9a-9c, 9b-9d and 7a-7b has two values of ϵ where $s_v = -1$. Thus the three families collectively have six bifurcations with three-dimensional orbits of twice the multiplicity of the planar orbit. Of greater interest for the present work are the three bifurcations with $s_v = 1$. These occur for $\epsilon = 0.032$ (family 9a-9c), $\epsilon = 0.047$ (9b-9d) and $\epsilon = 0.034$ (7a-7b), indicating bifurcations with three-dimensional orbits of the same multiplicity for eccentricities close to Jupiter's (0.048) are possible.

In marked contrast to vertical stability most orbits are orbitally unstable. Of the 35,417 orbits used to form the curves in the right hand plots Figure 9, only three are stable. These three are in the 9a-9c family and occur at and on either side of the maximum of ϵ (≈ 0.228). We also observe that increasing ϵ for families 9b-9d and 7a-7b usually leads to less instability. For family 9a-9c, the orbit 9a is more unstable than many of the orbits with $\epsilon > 0$ on the branch of the $\lambda_M(\epsilon)$ curve from the orbit 9a to the one with the maximum ϵ . A similar observation holds for orbit 9c. The variation of the instability with ϵ is far less for the remaining family 8a-8b.

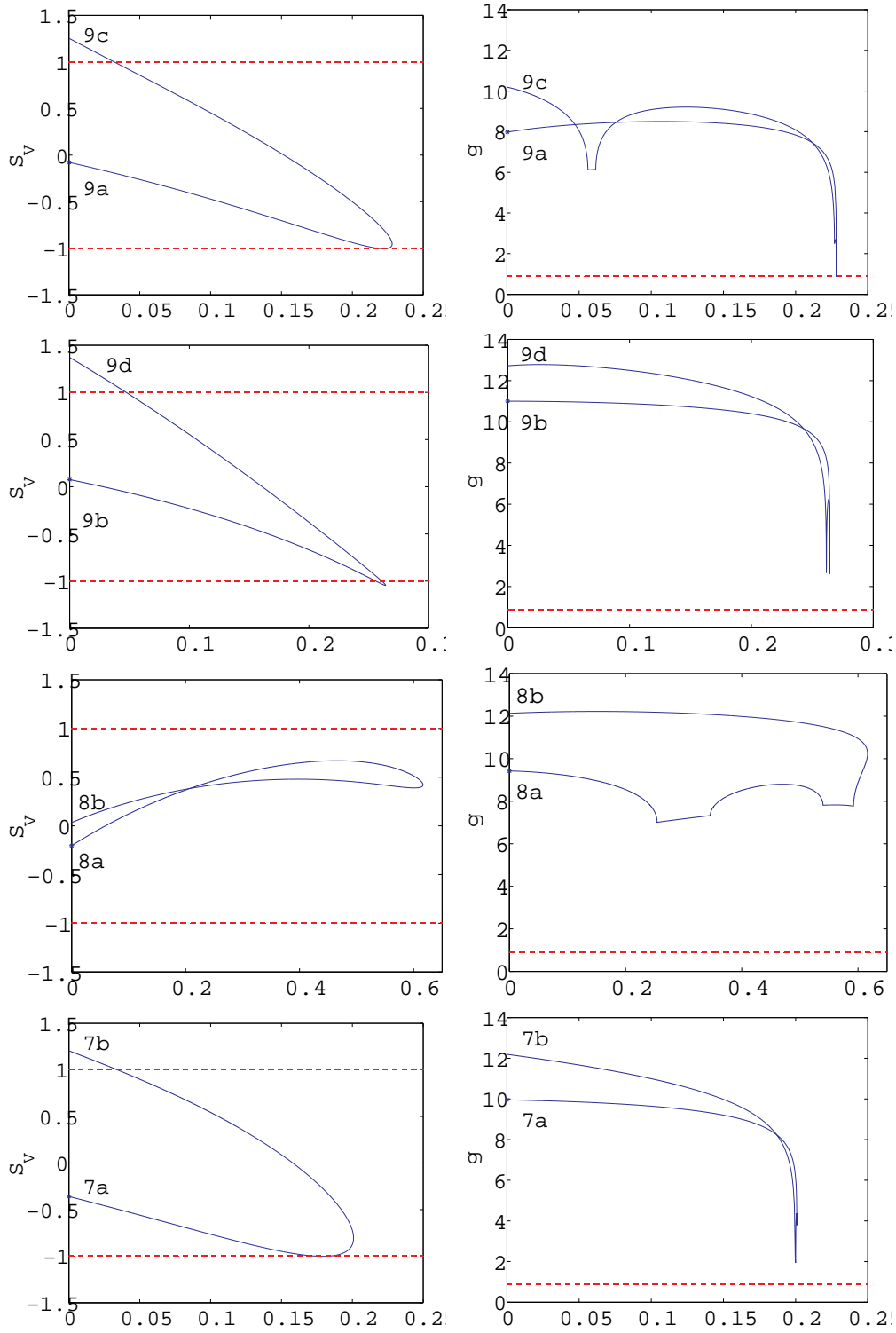


Figure 9: Stability plots for family 9a-9c (top), 9b-9d (top centre), 8a-8b (bottom centre) and 7a-7b (bottom). The ordinate of the left and right plots are s_v and $\gamma = \sinh^{-1} \lambda_M$ respectively. The abscissa for all plots is ϵ . The dotted lines are boundaries of regions of stability.

5 Discussion

We found families of horseshoe orbits for both the circular and elliptic R3BP with the Jupiter-Sun mass ratio, and investigated the stability and three-dimensional bifurcations of the new elliptic orbits.

We began by searching Taylor's [19] seven families of horseshoe orbits for the circular problem for bifurcations with elliptic orbits. As part of this work, we extended the continuations of Taylor. We found fourteen bifurcations with the number of bifurcations per family being zero, one, two or three. Once the bifurcations were located we continued on the eccentricity ϵ to find families of orbits for the elliptic problem. We found ϵ had turning points and this led to new families of horseshoe orbits for the circular problem. We performed continuation on these new families and this led to new families of elliptic horseshoe orbits and so on.

We investigated the stability of four families of elliptic orbits. We found most orbits were vertically stable but orbitally unstable. We also found that moving along a family in the direction of increasing ϵ often reduced the orbital instability. We examined the orbits of the four families more detail for eccentricities in a small interval about Jupiter's. We found bifurcations with three-dimensional orbits of the same multiplicity as the planar orbits. Bearing in mind the approximations inherent in the R3BP and the (small) long-term variation in Jupiter's eccentricity, our bifurcation analysis of the elliptic orbits shows the dynamics of horseshoe orbits in the Sun-Jupiter system could be appreciably more complex than modelled by the circular R3BP.

Acknowledgements

The authors thank the referee for detailed and constructive suggestions, particularly about the material on stability. Much of this work was done as part of the first author's fourth-year studies in Applied Mathematics at the University of Auckland. The first author thanks the second author for suggesting this project and for the help he gave throughout.

References

- [1] A. Abad, M. Arribas, A. Elipe, *On the attitude of a spacecraft near a Lagrangian point*, Bull. Astron. Inst. Czechosl., **40**, (1989), 302-307.
- [2] C.D. Bailyn, M.R. Garcia, J.E. Grindlay, *Outflow from the outer Lagrangian point: observations and models of 4U 2127+12 in M15*, Astroph. J., **344** (1989), 786-790.
- [3] T.A. Bray, C.L. Goudas, *Doubly symmetric orbits about the collinear Lagrangian points*, Astron. J., **72** 2 (1967), 202-213.
- [4] R. Buccheri, V. Salamone, K. Bennett, M. Busetta, L. Kuiper, W. Hermsen, M. McConnell, R. Much, J. Ryan, V. Schönfelder, H. Steinle, *Search for gamma-ray*

- emission from the Lagrangian points of PSR 1957+20*, *Astron. Astrophys. Suppl. Ser.*, **115** (1996), 305-309.
- [5] J.D. Hadjidemetriou, *The stability of periodic orbits in the three-body problem*, *Cel. Mech.* **12** (1975), 255-276.
- [6] M. Hénon, *Vertical stability of periodic orbits in the restricted problem*, *Astron. Astrophys.*, **28** (1973), 415-426.
- [7] C.J. van Houten, I. van Houten-Groeneveld, *Minor planets and related objects. V. The density of Trojans near the preceding Lagrangian point*, *Astron. J.*, **75** (1970), 5, 659 - 662.
- [8] O. Karlsson, *Transitional and temporary objects in the Jupiter Trojan area*, *Astron. Astrophys.*, **413** (2004), 1153-1161.
- [9] G. Katsiaris, *The Three-Dimensional Elliptic Problem*, in *Recent Advances in Dynamical Astronomy*, 3ed., B.D. Tapley, V. Szebehely (eds.), D. Reidel, Dordrecht-Holland, pp. 118-134, 1973.
- [10] J. Llibre, M. Ollé, *The motion of Saturn coorbital satellites in the restricted three-body problem*, *Astron. Astrophys.*, **378** (2001), 1087-1099.
- [11] V.V. Markellos, *Bifurcations of plane with three-dimensional asymmetric periodic orbits in the restricted three-body problem*, *Mon. Not. R. Astr. Soc.* **180** (1977), 103-116.
- [12] P. Oberti, *Lagrangian satellites of Tethys and Dione: II. theory of motion*, *Astron. Astrophys.*, **228** (1990), 275-283.
- [13] D. Pfenniger, *Stability of the Lagrangian points in stellar bars*, *Astron. Astrophys.*, **230** (1990), 55-66.
- [14] P.J. Prince, J.R. Dormand, *High order embedded Runge-Kutta formulae*, *J. Comput. Appl. Math.* **7** (1981), 67-76.
- [15] E. Rabe, *Determination and Survey of Periodic Trojan Orbits in the Restricted Problem of Three Bodies*, *Astron. J.*, **66** (1961), 9, 500-513.
- [16] I.A. Robin, *Bifurcations of Plane with Three-Dimensional Periodic Orbits in the Elliptic Restricted Problem*, *Celes. Mech.*, **23** (1981), 97-106.
- [17] S.D. Ross, W.S. Koon, M.W. Lo, J.E. Marsden, *Transport and capture of comets*, American Astronomical Society, DDA meeting, April 2001.
- [18] A.F. Schanzle, *Horseshoe-Shaped Orbits in the Jupiter-Sun Restricted Problem*, *Astron. J.*, **72** (1967), 2, 149-157.

- [19] D.B.Taylor, *Horseshoe Periodic Orbits in the Restricted Problem of Three Bodies for a Sun-Jupiter Mass Ratio*, *Astron. Astrophys.*, **103** (1981), 288-294.
- [20] P.A. Wiegert, K.A. Innanen, *An asteroidal companion to the Earth*, *Nature.*, **387** (1997), 685-686.
- [21] P.A. Wiegert, K.A. Innanen, S. Mikkola, *The Orbital Evolution of Near-Earth Asteroid 3753*, *Astron. J.*, **115** (1998), 2604-2613.
- [22] C.Zagouras, V.V. Markellos, *Axisymmetric Periodic Orbits of the Restricted Problem in Three Dimensions*, *Astron. Astrophys.*, **59** (1977), 79-89.
- [23] C.G. Zagouras, E.Perdios, O.Ragos, *New Kinds of Asymmetric Periodic Orbits in the Restricted Three-Body Problem*, *Astrophys. Space Sci.*, **240** (1996), 273-293.
- [24] S.-P. Zhang, K.A. Innanen, *A numerical investigation of the stability of Saturn's triangular Lagrange points*, *Astron. J.*, **96** (1988), 6, 1983 - 1988.
- [25] S.-P. Zhang, K.A. Innanen, *A numerical investigation of the stability of the triangular Lagrange points of the planets*, *Astron. J.*, **96** (1988), 6, 1989 - 1994.